Thin Solid Films 518 (2010) 17, 4997 – 5002, http://dx.doi.org/10.1016/j.tsf.2010.02.065

Influence of working pressure on ZnO:Al films from tube targets for silicon thin film solar cells

H. Zhu[1, 2,*], J. Hüpkes[2], E. Bunte[2], A. Gerber[2], S. M. Huang[1]

[1]Engineering Research Center for Nanophotonics and Advanced Instrument, Ministry of Education, East China Normal University, 200062, Shanghai, P. R. China

[2]Institute of Photovoltaics, Research Centre Jülich, D-52425 Jülich, Germany

[*]Corresponding author: Hongbing Zhu
e-mail: h.zhu@fz-juelich.de, tel.: +49-(0)2461-611550

Abstract

The mid-frequency magnetron sputtering of ZnO:Al layers from tube ceramic targets has been investigated for silicon solar cell application**.** The influence of working pressure on the structural, electrical and optical properties of sputtered ZnO:Al films was studied. ZnO:Al thin films with minimum resistivity of 3.4×10^{-4} Ω·cm, high mobility of up to 50 cm²/Vs and high optical transmission were prepared. The ZnO:Al microstructure and surface topography of wet-chemical etched ZnO:Al films was investigated. Depending on the sputter pressure we observed a gradual transition with reduction of grain and surface feature size upon etching that provided a method to optimize the light scattering properties. Silicon thin-film solar cells were prepared onto those films. High conversion efficiencies of up to 10.2 % were obtained for amorphous/microcrystalline silicon tandem solar cells.

Keywords: magnetron sputtering, ZnO:Al films, thin film silicon solar cells

1. Introduction

Aluminum doped Zinc Oxide thin films (ZnO:Al) are used as transparent conductive electrodes for thin film solar cells as well as other optoelectronic devices like light emitting

diodes (LEDs) and flat panel displays (FPDs). There are many fabrication methods for the preparation of the ZnO:Al thin films, such as magnetron sputtering [**2, 3**], sol-gel method [**5, 6**], etc.. High transparency and excellent conductivity are commonly reported [**1, 2, 3**]. Surface textured ZnO:Al thin films are of high interest for light trapping in thin film solar cells based on silicon [**4**].

In view on industrial application cost-effective processes at high deposition rates are required. High efficiency solar cells on sputter deposited and texture etched ZnO:Al films have been reported [**7, 8, 9, 10**]. However, so far best solar cell performance is still achieved by applying ZnO:Al front contacts, which were sputtered at low rates with radio frequency excitation from relatively expensive ceramic targets. Recently, cost-effective ceramic tube targets were developed. High quality zinc oxide films deposited from rotatable ceramic targets have been prepared with specific resistivity as low as 3.6×10^{-4} Ω·cm and microcrystalline silicon solar cells on such films were reported with efficiency of 8.5 % [**11**]. Nevertheless, performance and reliability of this technique need further comprehensive and systematic investigations before transferring to industrial environment.

This study focuses on the investigation of the influence of working pressure during magnetron sputtering of ZnO:Al thin films from rotatable dual magnetrons with ceramic targets. Electrical, optical and structural properties were investigated systematically. Additionally we report on the etching behavior and the resulting surface structures and light scattering properties. The performance of silicon thin film solar cells prepared on the ZnO:Al films after wet chemical etching were examined.

2. Experimental details

ZnO:Al films were prepared on glass substrates (Corning Eagle 2000) in an in-line sputtering system for 30 × 30 cm² substrate size (VISS 300, by von Ardenne Anlagentechnik,

Dresden, Germany). Two tube targets from $ZnO:Al_2O_3$ (99.5:0.5 wt%) ceramic material were mounted on rotatable magnetron cathodes. The size of both tube targets is 760 mm in length and 160 mm in diameter. About 10 mm thick target material is mounted on copper tubes. The distance between substrate and target surface is about 80 mm. The system was operated in mid frequency (MF) mode with an excitation frequency of 40 kHz for all ZnO:Al films. The substrates were heated in a loading chamber. The process chamber was held at a base pressure of less than 8×10^{-5} Pa. Pure argon was used as sputtering gas at flow rate of 200 sccm. The substrate temperature was kept constant at 350^{o} C for all films. If nothing else is given, the applied discharge power onto both cathodes was 2 kW in total. The working pressure was adjusted from 0.5 Pa to 3 Pa by throttle valves. After pre-sputtering for 5 min the substrates were coated in dynamic mode and the carrier moved forth and back in front of the rotating tube targets. A wet chemical etching step was carried out to get rough surface topography by dipping the samples into diluted hydrochloric acid (0.5 % HCl) at room temperature.

Film structure was studied by X-ray diffraction measurement in Bragg-Brentano geometry with copper K_α ray (λ=1.540560Å) excitation. The electrical properties of the ZnO:Al films were characterized by Hall-effect measurement using van der Pauw method (Keithley 926 Hall set-up). The thicknesses of all thin films were measured by a surface profiler (Dektak 3030 supplied by Veeco Instruments Inc.). Optical transmission and reflection measurement of surface textured thin films was carried out using a double beam spectrometer equipped with an integrating sphere (Perkin Elmer Lambda 19). An index matching fluid (CH_2I_2) was used to avoid systematic measurement errors due to light scattering of the rough films. The surface analysis of etched ZnO:Al thin films was carried out by atomic force microscopy (AFM).

Surface textured ZnO:Al films were applied as front contacts for single junction microcrystalline silicon p-i-n solar cells with an intrinsic layer thickness of about 1.1 µm as well as a-Si:H / µc-Si:H tandem solar cells. These cells were prepared using plasma enhanced chemical vapor deposition (PECVD). Details of silicon layer deposition and solar cell preparation are described elsewhere [**4**]. A ZnO:Al / Ag double layer served as back reflector. Before solar cell characterization thermal annealing of cells was done for 30 min at 160 ºC in order to form good contacts. Solar cell J-V characteristics were measured using a class A sun simulator at standard test conditions (AM1.5, 100 mW / cm^2 at 25ºC). Quantum efficiency measurement was carried out from 300 nm to 1100 nm at 25ºC.

3. Results

3.1 Deposition rate

The thickness of all as-deposited samples was between 780 nm and 900 nm. Fig.1 shows the dependence of the deposition rate on the working pressure. At low working pressure (0.5 Pa) the deposition rate is low and then increases with the escalated working pressure up to 1.0 Pa. Then the deposition rate decreases with increase of working pressure. The decay of deposition rate towards higher working pressure can be fitted according to Keller-Simmons model [**12, 13**]. The fit parameters are deposition rate prefactor R_0=16.8 nm·m/min and characteristic pressure-distance product $(pd)_0$= 55 Pa·cm. The value $(pd)_0$ is specific for the corresponding discharge and the geometric cathode environment. It describes the decay of deposition rate towards high pressures caused by a shielding effect of the gas particles between target and substrate. The low deposition rates at low working pressures was attributed to re-sputtering of ZnO by high energetic particles, which would be more prevalent at lower pressures [**14**]. The characteristic pressure-distance product of $(pd)_0$ = 55 Pa·cm is quite high and the corresponding decay flat as compared to reports on other materials [**13**] and other process conditions [**14, 15**]. We suggest, that the high value of $(pd)_0$ is related to the

specific geometry of the tube targets and cathode environment as well as other process conditions.

3.2 Structural properties

The XRD measurements show a strong and narrow (002) peak at about 34.50º for all investigated samples. All other peaks are suppressed due to the strong texture of the ZnO:Al films. Thus, we restrict the evaluation on width and position of the (002) peak. The exact peak positions and full width at half maximum (FWHM) of (002) peak of these ZnO:Al thin films as a function of working pressure are shown in **Fig. 2**. The (002) peaks are observed at positions between 34.47º and 34.52º. There is no significant dependency on the working pressure observed. This indicates that bombardment of the growing films with high energetic oxygen ions is not relevant in the investigated working pressure range [**14**]. FWHM increases slightly with high working pressure in the range from 0.17 º to 0.19 º, which corresponds to a smaller grain size of the film at high working pressure. According to Scherrer formula [**16**], the grain sizes of these ZnO films are between 53-59 nm. The decreased grain size with increasing working pressure is caused by thermalization of the sputtered particles at high pressure by collisions in the plasma. Thus, the adatoms have only limited energy for surface diffusion [**Thornton**]. Even though, the grain size is much smaller than film thickness, the large grains reveal ZnO:Al films of high crystalline quality as compared to other publications [**2, 3, 7, 14**].

3.3 Electrical properties

Fig. 3 shows the electrical properties of as-deposited ZnO:Al thin films as a function of working pressure. The resistivity (open circles) of the as-deposited ZnO:Al films initially decreases and then increases with the increase of the working pressure from 0.5 Pa to 3 Pa. A minimum resistivity value of $3.4 \times 10^{-4}\ \Omega \cdot \mathrm{cm}$ was obtained at 1.5 Pa.

Carrier concentration (solid squares) and Hall mobility (open triangles) of the films are given on additional y-axis in **Fig. 3**. Note that the error of Hall data is about 10%. The carrier concentration *n* is between 3.3 $\times 10^{20}$ cm^{-3} and 4.2 $\times 10^{20}$ cm^{-3} without significant trend, while the Hall mobility μ_H of the films exhibited a significant maximum value at about 1-1.5 Pa. A very high mobility value 50 cm^2/Vs was obtained for the sample deposited at 1 Pa.

Moreover, we also added the corresponding data of one ZnO:Al thin film deposited at 14 kW discharge power into **Fig. 3**, which are very close to values of the thin film deposited at lower discharge power. Due to the high discharge power the deposition rate raised by a factor of 7. Typically, one would expect stronger ion bombardment and worse electrical properties at these conditions, but our data illustrates that high quality ZnO:Al thin films can be prepared at high deposition rate.

3.4 Morphology

All the samples exhibit milky surface after wet chemical etching in the 0.5% HCl for 50 seconds. Various crater-like and hill-like surface features were etched into ZnO:Al films. The AFM images shown in **Fig. 4** exhibit the systematic influence of the working pressure on the surface morphology of etched ZnO:Al thin films. As the deposition pressure increases, the lateral size and depth of formed craters decrease. **Fig. 5** shows statistical analysis of the surface features by the surface inclination angle (left axis, solid black symbols) and crater density (right axis, open red symbols). The inclination angle is evaluated as angle of the normal vector of the local ZnO surface in respect to the overall normal vector of mean surface level (z-axis) [**25**,**26**]. The inclination angle decreases from 28 ° at low pressure to 15 ° at 1.5 Pa. This sample exhibits shallow craters. For high sputter pressure the inclination angle

increases continuously to about 40°. At low pressure of less than around 1 Pa the corresponding feature size is 1-2 µm in lateral direction and 450 nm in depth. The craters are regularly distributed over the surface. At high pressures, the features become much smaller with an average size of 0.1-0.2 µm in lateral direction and 100 nm in depth. Consequently, the crater density (**Fig 5)** continuously rises from less than 1 μm^{-2} to more than 5 μm^{-2}.

Fig. 6 presents root mean square (RMS) roughness and etch rate of the ZnO:Al films deposited with different pressures. The RMS roughness of the etched thin film decreases from 170 nm to 70 nm as the working pressure increases from 0.5 Pa to 3 Pa. The etched film deposited at 1.5 Pa shows a RMS roughness value which deviates from the general trend. The etch rate increases from 2.7 nm/s to 6.5 nm/s when increasing the deposition pressure from 0.5 Pa to 3 Pa. In other words, lower working pressure leads to more etch resistant ZnO:Al films and higher RMS roughness. Other publications report an increased RMS roughness after longer etching resulting in removal of more material [**27**]. This effect is not the major effect here, since the amount of removed material is much higher for smoother films due to the constant etch duration at increased etch rate. The roughness effect is mainly attributed to the large feature size at low pressure.

3.5 Optical properties

Fig. 7 shows the optical transmission and absorption of texture etched films sputtered at different working pressures. Between 400nm and 800nm all investigated films show almost 90% transmission and very small absorption. In **Fig. 8** the transmission and absorption at 800 nm and 1200 nm wavelength are shown. In the long wavelength range, it is found that the samples deposited above about 2 Pa show a higher transmission and lower absorption than those of other three. This part of the spectrum is influenced by the carrier concentration and

the film thickness. Due to the different etch rates, the film thicknesses after etching vary. Thus, both effects may play a significant role.

The resulting haze, defined as quotient of diffuse and total transmission, is shown in **Fig. 9** for etched ZnO:Al thin films deposited at different working pressure. It can be noted that light scattering is stronger for short wavelength, meaning that only very rough films have considerable haze in the near infrared spectral range. For higher deposition pressures the haze decreases due to the already described decrease of structure size shown in **Figs. 4** and **6**. In the wavelength range from 400 to 1300 nm, for a fixed wavelength, the haze decreases with the increasing working pressure except the sample deposited at 1.5 Pa. It shows a very flat surface (see **Fig. 4(c)**) and the smallest RMS roughness of 63 nm. **Fig. 10** (left axis) exhibits Haze at 700 nm as function of RMS roughness. Within this series haze increases with RMS roughness linearly from 0.15 to more than 0.7. This is expected from scalar scattering theory [paper, check Schulte phd thesis].

3.6 Solar cells

The most sensitive detector to evaluate the suitability of texture etched ZnO:Al layers for the application in solar cells is the solar cell itself. Therefore etched ZnO:Al layers with different surface morphology were applied as front contact in single junction µc-Si:H p-i-n solar cells and a-Si:H /µc-Si:H tandem solar cells. Single junction microcrystalline silicon µc-Si:H p-i-n solar cells with an intrinsic layer thickness of ~1.1 µm were co-deposited on the etched ZnO:Al thin films. The corresponding solar cell parameters efficiency, fill factor (FF), short circuit current density (J_{SC}) and open circuit voltage (V_{OC}) are shown in **Table 1**. The highest short circuit current density J_{SC} of 23.3 mA/cm^2 was achieved for the ZnO film deposited at 0.5 Pa. This layer exhibits the largest craters and highest RMS roughness. For most samples of our series the obtained J_{SC} results follow the trend of increasing current

density with increasing haze (see **Fig. 10**, right axis). Also the haze at 700 nm of these ZnO:Al films increase with RMS roughness (**Fig. 10**). Note that the observed relation of RMS, haze and J_{SC} is not generally valid and strongly depends on shape and size of surface features [**28**]. Wide and deep craters are beneficial for efficient light trapping effect [**1, 2**].

The correlation between the deposition pressure of ZnO:Al films on FF and V_{OC} of solar cells is shown in Table I. The deposition pressure during sputtering of ZnO:Al does not influence the solar cell performance directly of course, but an indirect influence via the etched surface structures can be oserved. FF and V_{OC} have a maximum value of 72.1 % and 521 mV, respectively, at 1.5 Pa and decrease both at lower and higher pressures. For the ZnO:Al films deposited at the working pressure of more than 1.5 Pa and with small and steep craters, low FF values of 64-65 % and low V_{OC} of 492-496 mV were observed. Possible reasons for this behavior are on the one hand, steep craters could favor shunts. On the other hand, the different surface texture may affect the growth of silicon layers that lead to deterioration of the silicon layers. As a result, the highest conversion efficiency η of 8.5 % and a high short current density of 22.9 mA/cm^2 were obtained for solar cells on ZnO:Al layers deposited at 1 Pa. The short circuit current density was confirmed by quantum efficiency measurement as shown in **Fig. 11** (red, dashed line). Moreover, TCO layers deposited at 1 Pa were used for preparation of a-Si:H/µc-Si:H tandem solar cells with a-Si:H top cell thickness of about 300nm and µc-Si:H bottom cell of about 1.1 µm. From quantum efficiency measurements (see **Fig. 11**) a top and bottom cell photocurrent of 10.7 mA/cm^2 and 11.5 mA/cm^2 was derived, respectively. Thus, the tandem cell is top limited and a better utilization of the sun spectrum is possible by tuning the absorber layer thicknesses. The IV measurements of the tandem cells under DC solar simulator have shown current collection. Thus, the top cell current of 10.7 mA/cm^2 was assumed for the calculation of the tandem cell efficiency, which is 10.2%.

4. Discussion

In previous works, the sputter parameters deposition pressure and substrate temperature were found to have a major influence on the material properties of ZnO:Al films sputter deposited from ceramic or metallic targets in static as well as in in-line mode [**8, 9, 17, 18, 19**]. Resistivities below 5 $\times 10^{-4}$ Ω·cm were achieved at sputter pressures below a typical value, that varies between 0.3 Pa and 4 Pa depending on other deposition conditions [**8**]. Typically for DC or MF excitation and at high substrate temperatures the transition from low- to high-ohmic films occurs at higher pressures compared to the RF case and low temperatures, respectively. From **Fig. 3** one can see, that the range of deposition pressure in our process yielding conductive films with the resistivity below 5 $\times 10^{-4}$ Ω·cm is also very wide. The transition from relatively low- to high-ohmic films would occur beyond 3 Pa. The wide range of low resistivity seems be related to the high characteristic pressure-distance product $(pd)_0$ from the fit of deposition rate dependence. The trend of mobility μ_H and carrier density n at low working pressure during our processing may be related to the energetic negative oxygen ions bombardment effect, resulting in intrinsic stress and defects that compensate active dopants [**21, 22, 23, 24**]. Even though, XRD results do not point towards increased intrinsic stress at low pressure, the decreased deposition rate is an indication for the bombardment and electrical properties are more sensitive to damage. As the working pressure increases above 1 Pa, energetic oxygen ion bombardment can be ignored [**21, 23, 24**]. Thermalization by collisions in the plasma of sputtered particles at high pressure reduce the energy for surface diffusion [**17**]. Despite of the trends observed for electrical properties, all ZnO:Al films show excellent electrical properties with very low resistivity (below 4.5 $\times 10^{-4}$ Ω·cm) and excellent mobility values above 40 cm²/Vs. The high ZnO:Al quality is further supported by the large grain size extracted from XRD data.

The obtained minimum resistivity of 3.4 $\times 10^{-4}$ Ω·cm reveals the high quality of our ZnO:Al films comparable to previous results. The high mobility of 50 cm²/Vs even exceeds

most values reported previously for high mobility ZnO:Al films [**2, 10, 20]** The maximum of mobility and carrier concentration nearly coincide at about 1 Pa. This reveals, that hall mobility of this ZnO:Al film series is not limited by ionized impurity scattering [**20**] which is caused by high doping level and the different structural film properties that lead to different grain boundary scattering and other scattering mechanisms.

Characteristic surface features were observed in RF and reactively DC sputtered ZnO:Al films after the wet etching [**1, 2, 8**]. No matter of deposition technique the surface features for sputtered ZnO:Al films after etching in diluted HCl strongly depend on deposition conditions. Previous publications describe three types of surface textures after etching in dependence on working pressure and substrate temperature and a structure zone model based on Thornton model was introduced [**8, 9**]. In our work, we observed a continuous transition from relatively large craters to small features with increasing working pressure as seen in **Fig. 4**. From our observations we conclude, that our films form a transition from Type B structures with regular large craters to Type A with very small features, as introduced by Kluth et al [**8**]. This continuous and wide transition zone was never reported before. However, there is no structure type, that can be identified as real Type A and also there are no structures of Type C. These types are expected to occur at even higher and lower pressures, respectively. Also other ZnO:Al film properties like etch rate and XRD results follow the trends described by the model.

A detailed microscopic model for the etching behavior and the formation of craters is not available yet. Owen et al [Owen, MRS] described that the etching of craters starts at certain points of attack. At these points the ZnO surface is etched and craters evolve, while other surface areas are not harmed by the acid. The reason for the acid picking these points and the subsequent evolution of craters is ascribed to ‘peculiar defects’. Even though it seems likely, a

correlation between structural properties and etching behavior could not be found so far. For the investigated films, a decrease of the grain size with increasing working pressure was identified by XRD measurements. On the other hand the wet-chemical etching results in smaller surface features for ZnO:Al films sputtered at higher pressures. This may give a first hint that peculiar defects are related to certain grains or grain boundaries and the peculiar defect density is directly related to the density of grains or grain boundaries.

5. Summary

MF magnetron sputtering using ceramic tube targets has been investigated for preparation of transparent and conductive zinc oxide layers for silicon solar cell application**.** The influence of working pressure on the structural, electrical and optical properties of sputtered ZnO:Al films by this technology was investigated. ZnO:Al thin films with minimum resistivity of 3.4 $\times 10^{-4}\,\Omega\cdot$cm, very high mobility of 50 cm²/Vs and high optical transmission were obtained. A wet chemical etching step was carried out by dipping the as-deposited samples into diluted hydrochloric acid (0.5 % HCl) at room temperature. We found similarities to structure zone model introduced by Kluth et al, but additionally we observed a new broad transition zone. The obtained textured ZnO:Al films were applied as front contacts both for single junction microcrystalline silicon p-i-n and tandem solar cells. High conversion efficiencies up to 8.5 % were obtained for p-i-n microcrystalline silicon solar cells and a high short circuit current of 10.7 mA/cm^2 for tandem solar cells based on the optimized ZnO:Al films was extracted by quantum efficiency measurement, respectively, leading to an efficiency well above 10 %.

Acknowledgment

The authors would like to thank H. Siekmann, J. Worbs, J. Kirchhoff, W. Reetz, W. Appenzeller, S. Jorke and R. van Aubel for extensive technical support. The authors thank A.

Gerber and A. Gordijn for fruitful discussions. Financial support by the German BMU (contract no. 0327693A) and by the European Commission (contract no. 019670**)** is gratefully acknowledged. The authors also thank the company W. C. Heraeus for providing the targets.

References

[1] J. Müller, G. Schöpe, O. Kluth, B. Rech, M. Ruske, J. Trube, B. Szyszka, X. Jiang, G. Bräuer. Thin Solid Films 392 (2001) 327.

[2] M. Berginski, J. Hüpkes, M. Schlute, G.. Schöpe, H. Stiebig, M. Wuttig. J. Appl. Phys. 101 (2007) 074903-1.

[3] J. Hüpkes,B. Rech, S. Calnan, O. Kluth, U. Zastrow, H. Siekmann, M. Wuttig. Thin Solid Films 502 (2006) 286.

[4] B. Rech, T. Repmann, V. M. N. van den Donker, M. Berginski, T. Kilper, J. Hüpkes, S. Calnan, H. Stiebig, S. Wieder. Thin Solid Film 511-512 (2006) 548.

[5] M. J. Alam and D. C. Cameron. J. Vac. Sci. Technol. A. 19 (2001) 1642.

[6] W. Tang and D. C. Cameron. Thin Solid Films. 238 (1994) 83.

[7] C. Agashe, O. Kluth, J. Hüpkes, U. Zastrow and B. Rech. J. Appl. Phys.95 (2004) 1911.

[8] O. Kluth, G.. Schöpe, J. Hüpkes, C. Agashe, J. Müller, B. Rech. Thin Solid Films 442 (2003) 80.

[9] J. Hüpkes, B. Rech, O. Kluth, T. Repmann, B. Zwaygardt, J. Müller, R. Drese, M. Wuttig. Sol. Energy. Mater. Sol. Cells 90 (2006) 3054.

[10] B. Szyszyka. Thin Solid Films 351 (1999) 164.

[11] H. Zhu, E. Bunte, J. Hüpkes, H. Siekmann, S. M. Huang. Thin Solid Films 517 (2008) 3161.

[12] J. H. Keller, R. G. Simmons. IBM J. Res. Develop.23 (1979) 24.

[13] T. P. Druesedau, M. Loehman and B. Garke. J. Vac. Sci. Technol. A 16(1998)2728.

[14] O. Kappertz, R. Drese, J. M. Ngaruiya, M. Wuttig. Thin Solid Films 484 (2005) 64.

[15] J. Hüpkes, Ph.D. Thesis, Institute of Photovoltaic, Research center Jülich, Germany, 2006.

[16] L.V. Azaroff. Elements of X-ray Crystallography, Mcgraw-Hill, New York, 1968.

[17] K. H. Kim, K. C. Park, D. Y. Ma. J. Appl. Phys 81 (1997) 7764.

[18] J. F. Chang, M. H. Hon. Thin Solid Films. 386(2001)79.

[19] A. Löffl, S. Wieder, B. Rech, O. Kluth, C. Beneking, H. Wagner. Proceedings of the 14th European PV Solar Energy Conference, Barcelona, Spain, 1997, p. 2089.

[20] T. Minami, H. Nanto and S. Takata. Jpn. J. Appl. Phys 24 (1985) L781.

[21] I. Petrov, V. Orlinov, A. Misiuk. Thin Solid Films 120 (1984) 55.

[22] T. Minami, H. Nanto and S. Takata. Jpn. J. Appl. Phys 23 (1984) L280.

[23] K. Tominaga, K. Kuroda and O. Tada. Jpn. J. Appl. Phys 27 (1988) 1176.

[24] J. Hinze and K. Ellmer. J. Appl. Phys 88 (2000) 2443.

[25] H. Stiebig, M. Schulte, C. Zahren, C. Haase, B. Rech, P. Lechner, Proc. SPIE 6197 (2006) 1

[26] M. Schulte, S. Jorke, C. Zahren, H. Hüpkes and H. Stiebig. 22nd European Photovoltaic Solar Energy Conference, 3-7 September 2007, Milan, Italy, p 2190.

[27] O. Kluth, C. Zahren, H. Stiebig, B. Rech and H. Schade. 19th European Photovoltaic Solar Energy Conference, 2004, Paris, France, p 1587.

[28] P. Lechner, R. Geyer, H. Schade, B. Rech, O. Kluth and H. Stiebig. 19th European Photovoltaic Solar Energy Conference, 2004, Paris, France, p 1591.

Figure captions

Fig.1. Dependence of deposition rate on working pressure. The solid curve is a fit according to Keller-Simmons model [**13**].

Fig.2. Positions of (002) peak and full width at half maximum (FWHM) of XRD patterns of ZnO:Al thin films deposited at different working pressure. The line is the guide to the eyes.

Fig.3. Electrical properties of ZnO:Al thin films deposited at different working pressure and of one ZnO:Al thin film deposited at 14 kW. The lines are the guide to the eyes.

Fig.4. AFM pictures of etched ZnO:Al thin films deposited at different working pressure: (a) 0.5 Pa, (b) 1 Pa, (c) 1.5 Pa, (d) 2 Pa, (e) 2.5 Pa and (f) 3 Pa.

Fig.5. Dependence of inclination opening angle and crater density on the working pressure.

Fig.6. RMS roughness and etching rate of texture-etched ZnO:Al thin films deposited at different working pressure.

Fig.7. Transmission and absorption of ZnO:Al thin films deposited at different working pressures.

Fig.8. Average transmission and absorption at 800nm ± 20 nm and 1200nm ± 20 nm of ZnO:Al thin films deposited at different working pressures.

Fig.9. Spectral haze of ZnO:Al thin films deposited at different working pressure.

Fig.10. Haze at 700 nm of ZnO:Al thin films and J_{SC} of single junction μc-Si:H p-i-n solar cells on these thin films as substrate versus RMS roughness.

Fig.11. Quantum efficiency of the tandem solar cell on optimum thin film**.**

Table 1. Performance of single junction μc-Si:H p-i-n solar cells.

Zhu_Fig.1

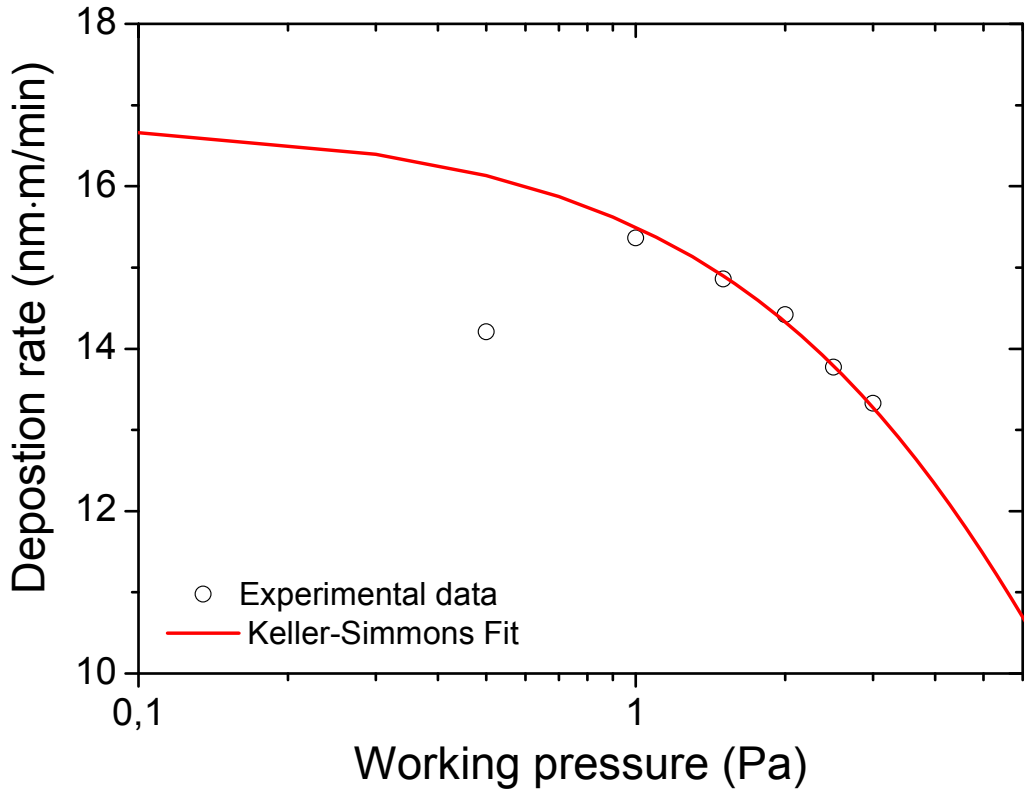
18
16
14
12
10
Depostion rate (nm·m/min)
0,1
1
Working pressure (Pa)
Experimental data
Keller-Simmons Fit

Zhu_Fig.2

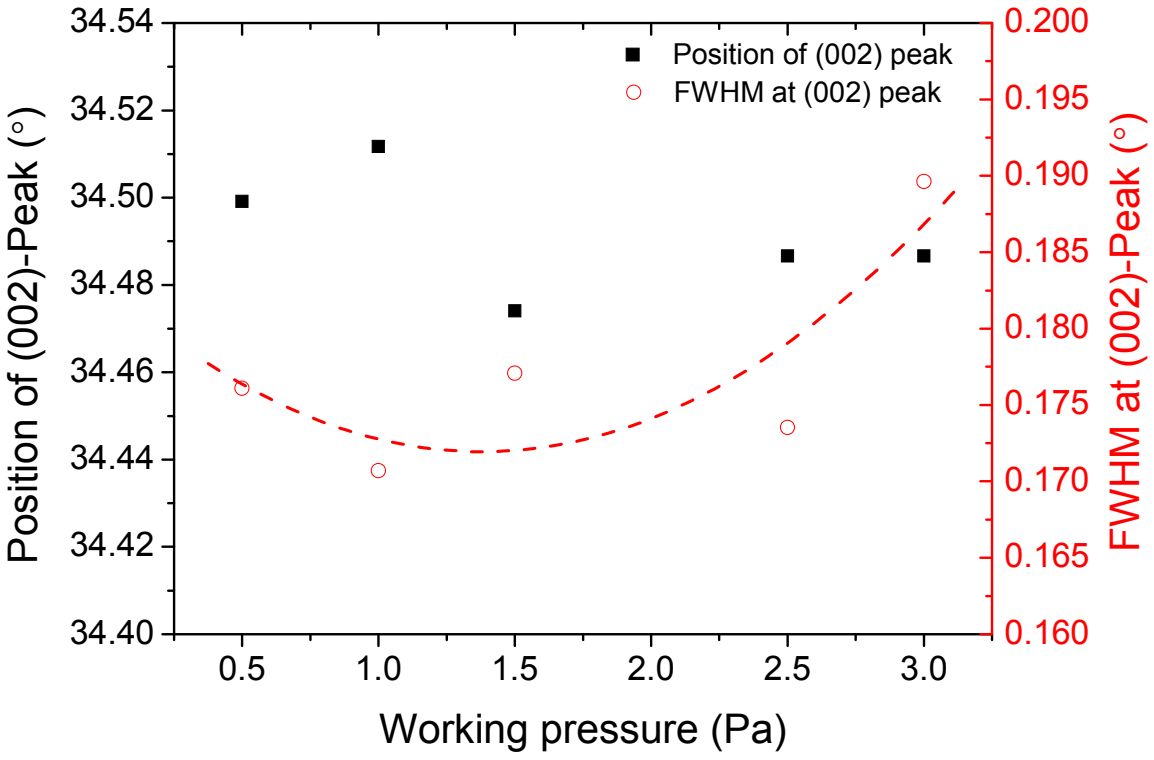
Position of (002) peak
FWHM at (002) peak
Position of (002)-Peak (°)
FWHM at (002)-Peak (°)
Working pressure (Pa)
34.54
34.52
34.50
34.48
34.46
34.44
34.42
34.40
0.200
0.195
0.190
0.185
0.180
0.175
0.170
0.165
0.160
0.5
1.0
1.5
2.0
2.5
3.0

Zhu_Fig.3

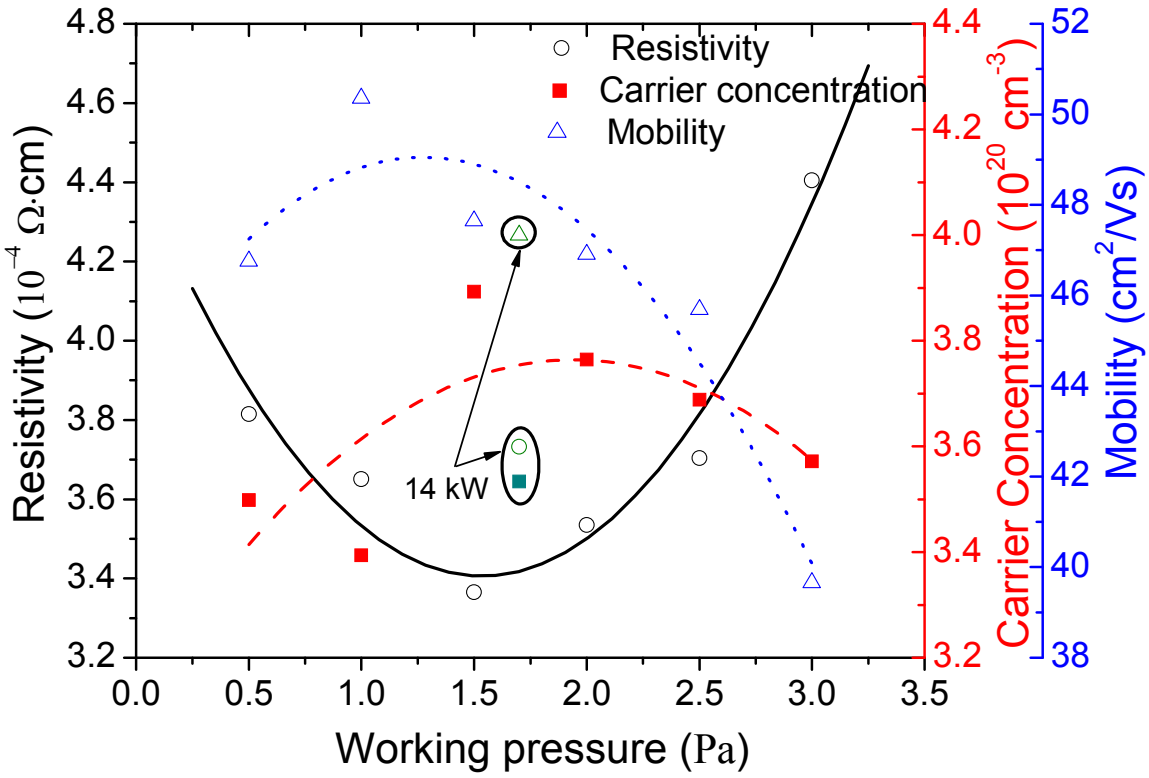
Resistivity
Carrier concentration
Mobility
14 kW
Resistivity (10^{-4} Ω·cm)
Carrier Concentration (10^{20} cm^{-3})
Mobility (cm^2/Vs)
Working pressure (Pa)
4.8
4.6
4.4
4.2
4.0
3.8
3.6
3.4
3.2
4.4
4.2
4.0
3.8
3.6
3.4
3.2
52
50
48
46
44
42
40
38
0.0
0.5
1.0
1.5
2.0
2.5
3.0
3.5

Zhu_ Fig.4 (a)

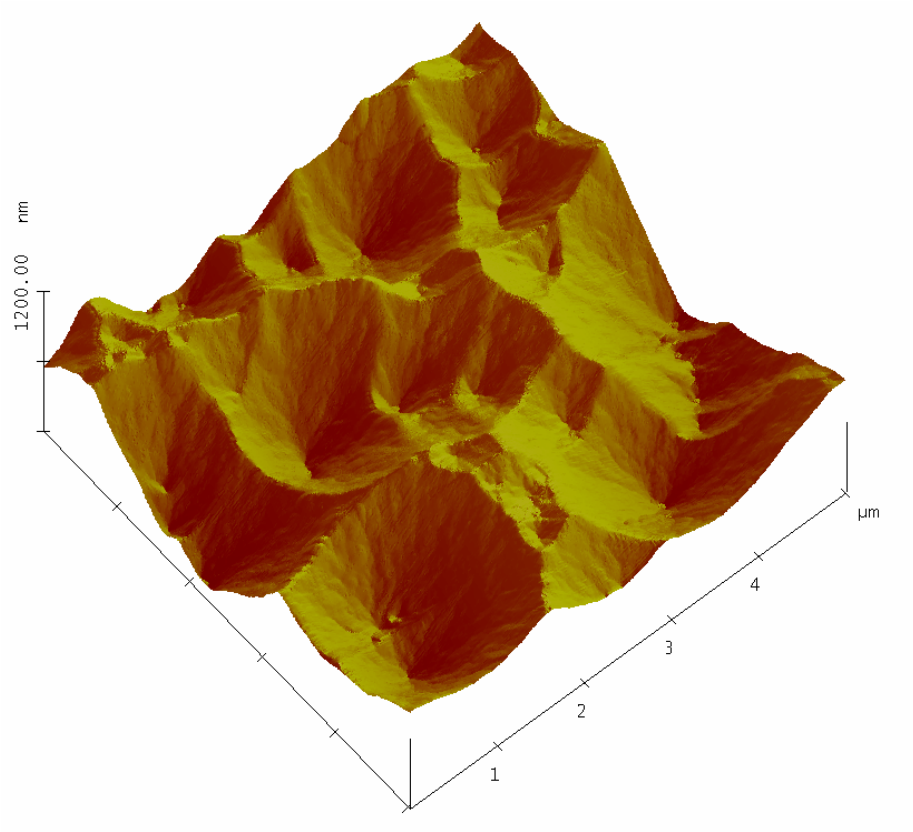

Zhu_Fig.4 (b)

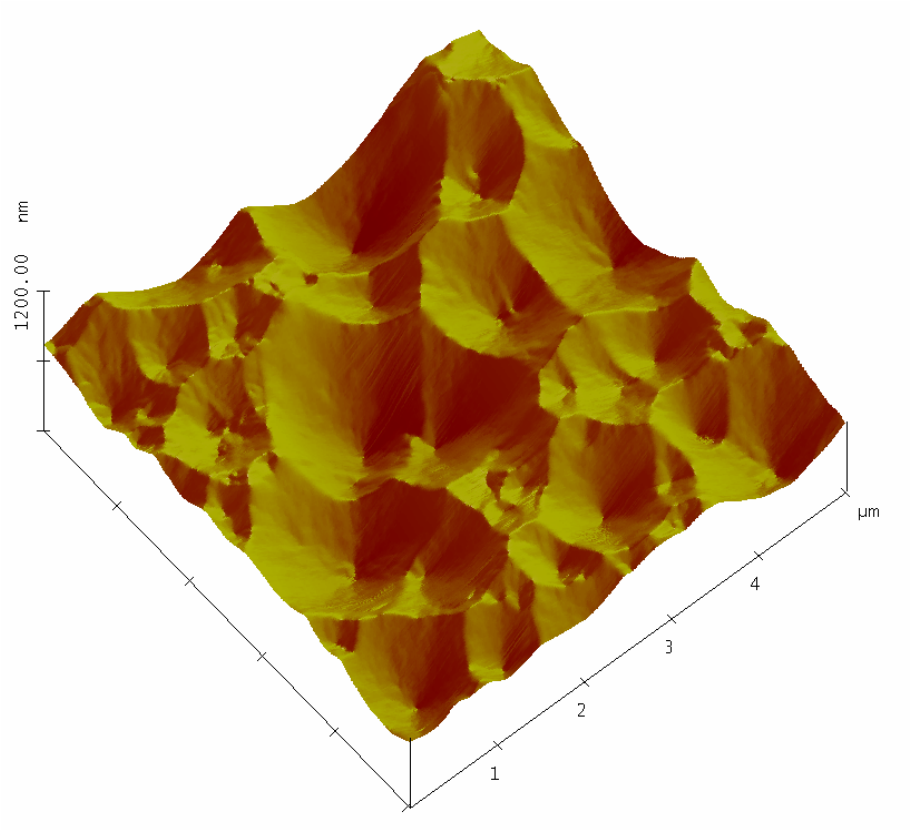

Zhu_Fig.4 (c)

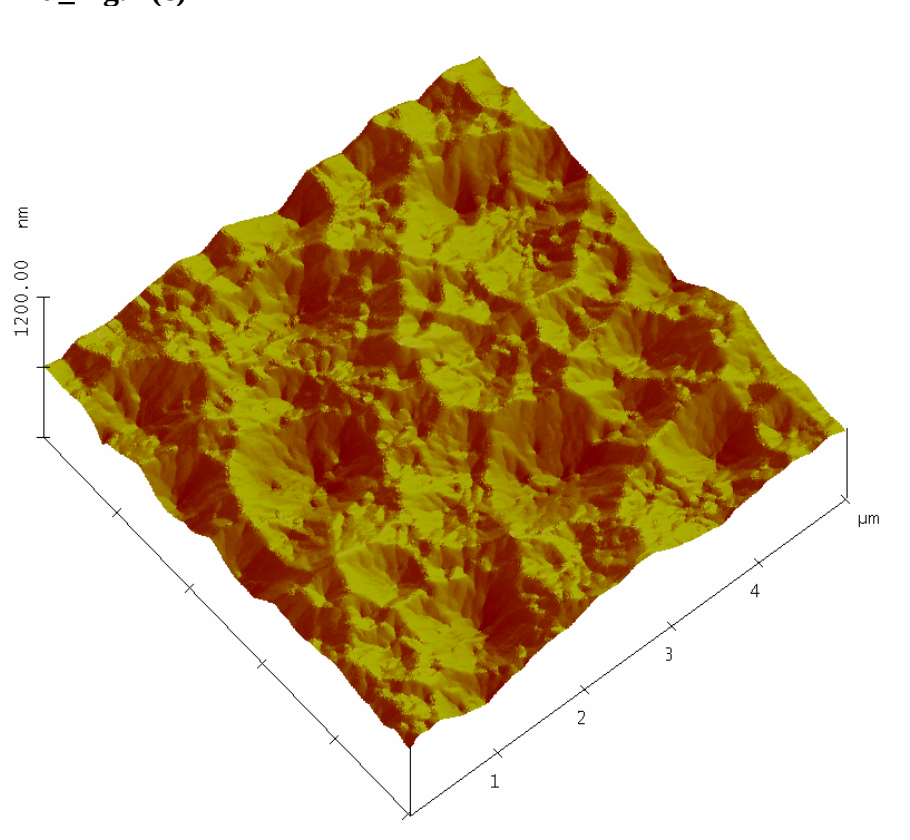

Zhu_Fig.4 (d)

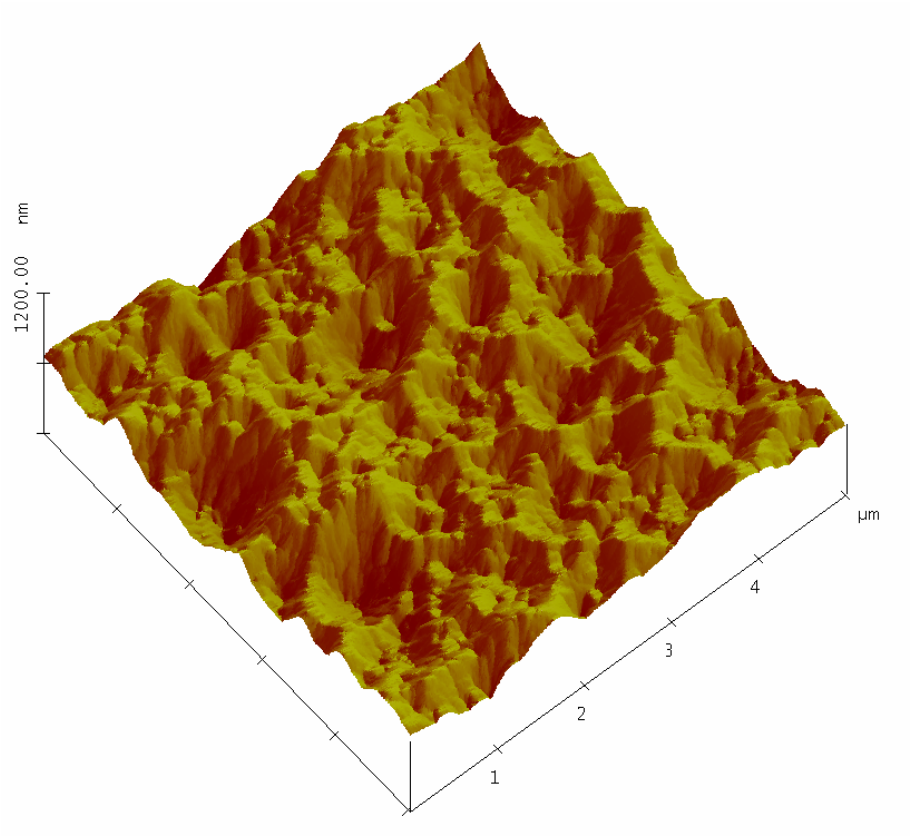

Zhu_Fig.4 (e)

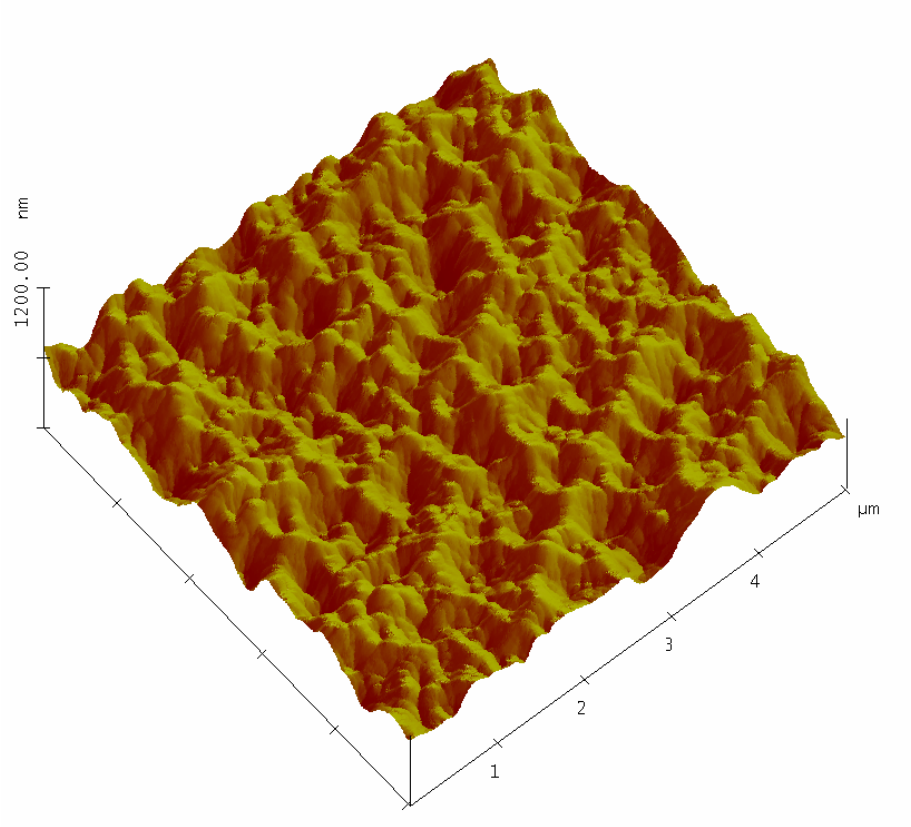

Zhu_Fig.4 (f)

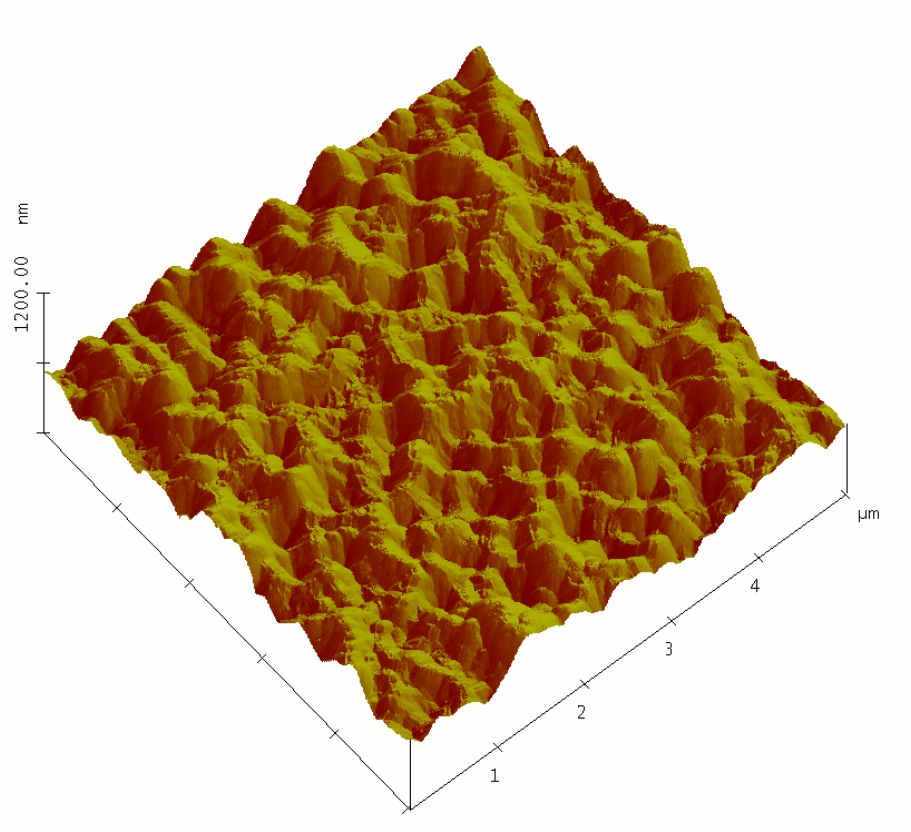

Zhu_Fig. 5

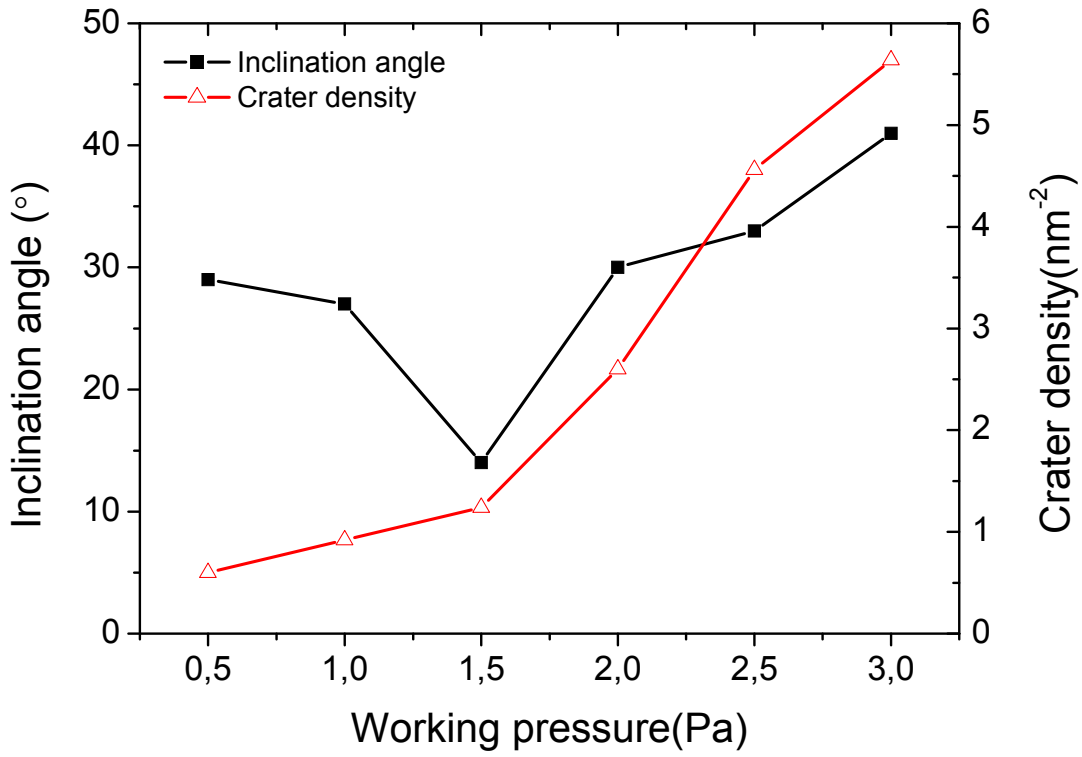
Inclination angle
Crater density
Inclination angle (°)
Crater density(nm-2)
Working pressure(Pa)
0
10
20
30
40
50
0
1
2
3
4
5
6
0,5
1,0
1,5
2,0
2,5
3,0

Zhu_Fig. 6

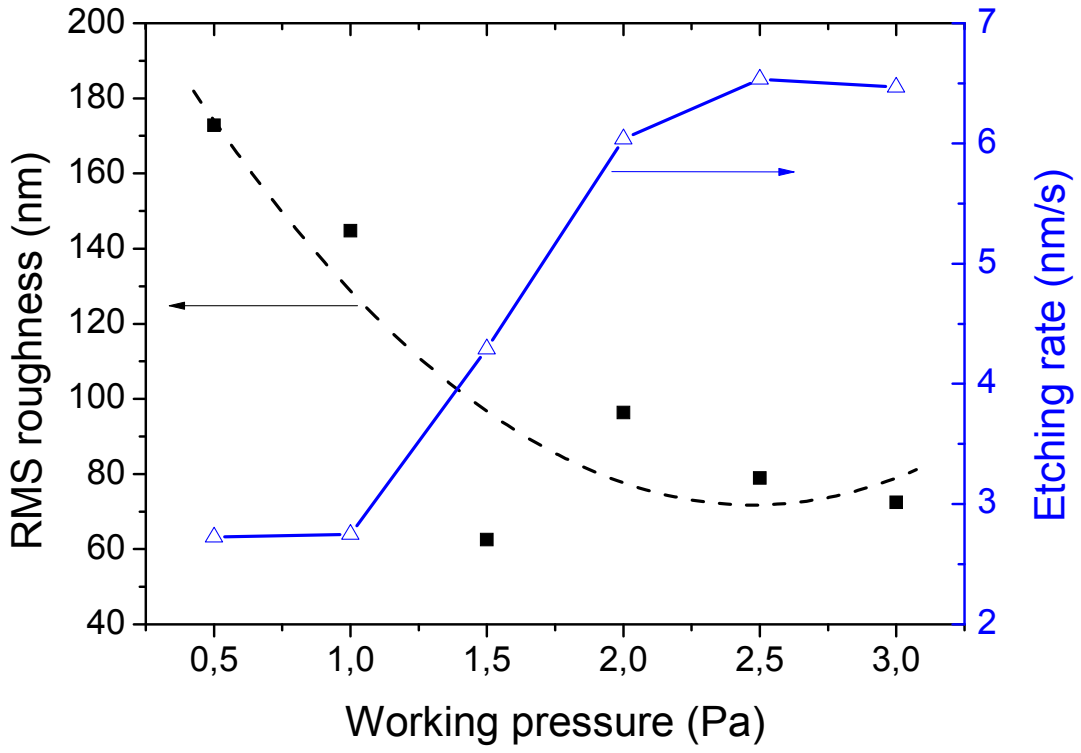
RMS roughness (nm)
Etching rate (nm/s)
Working pressure (Pa)
200
180
160
140
120
100
80
60
40
7
6
5
4
3
2
0,5
1,0
1,5
2,0
2,5
3,0

Zhu_Fig. 7

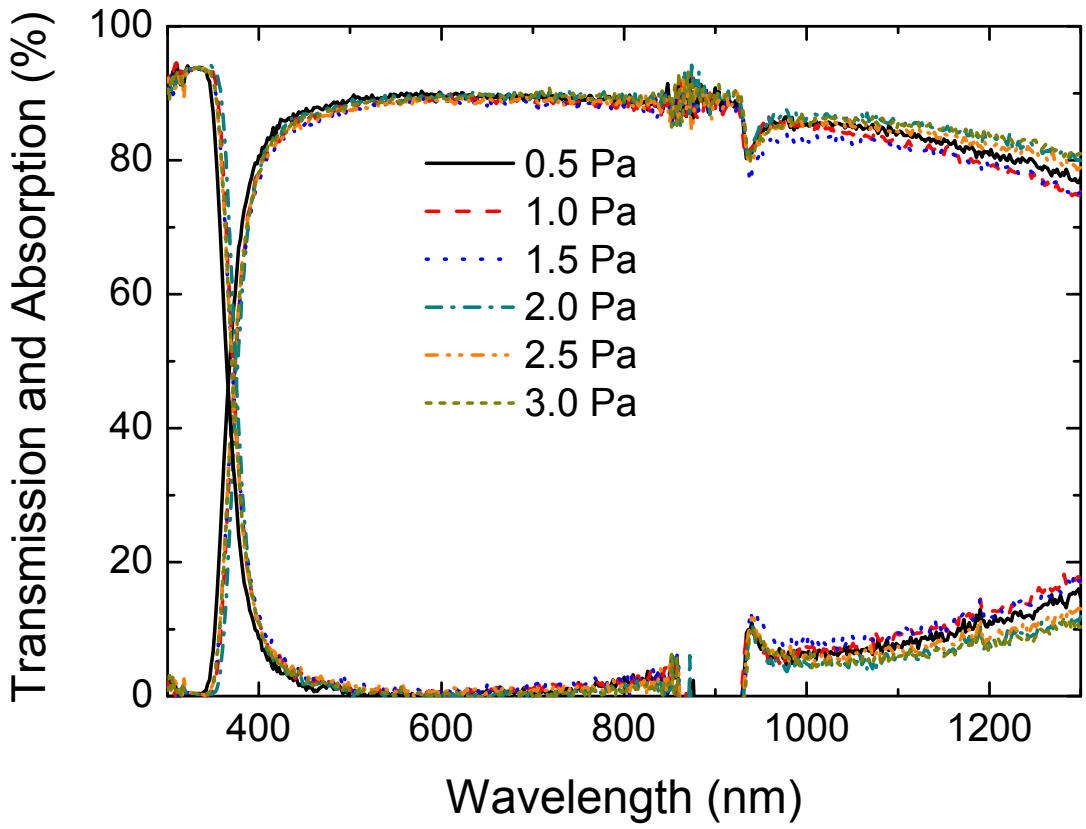
Transmission and Absorption (%)
Wavelength (nm)
0.5 Pa
1.0 Pa
1.5 Pa
2.0 Pa
2.5 Pa
3.0 Pa
0
20
40
60
80
100
400
600
800
1000
1200

Zhu_Fig. 8

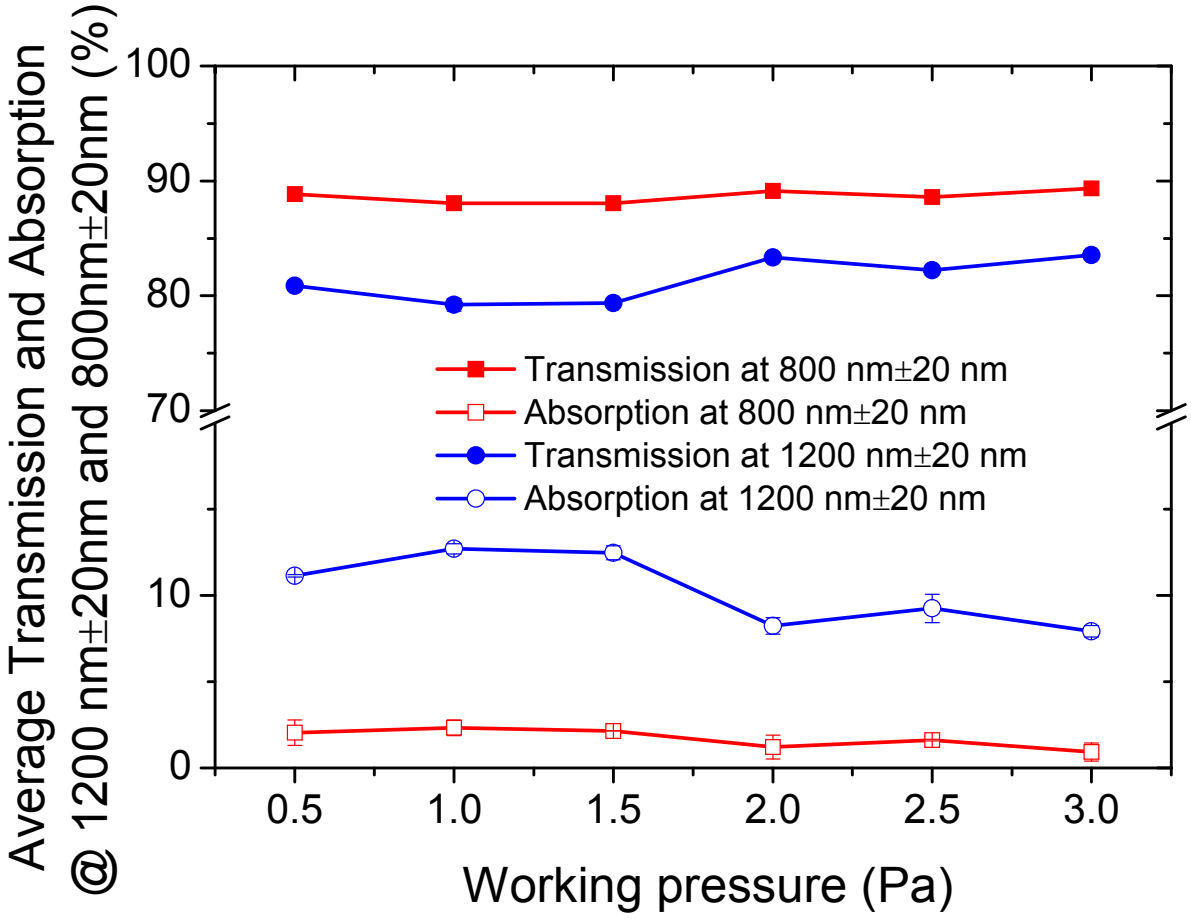
Average Transmission and Absorption @ 1200 nm±20nm and 800nm±20nm (%)
100
90
80
70
10
0
0.5
1.0
1.5
2.0
2.5
3.0
Working pressure (Pa)
Transmission at 800 nm±20 nm
Absorption at 800 nm±20 nm
Transmission at 1200 nm±20 nm
Absorption at 1200 nm±20 nm

Zhu_Fig. 9

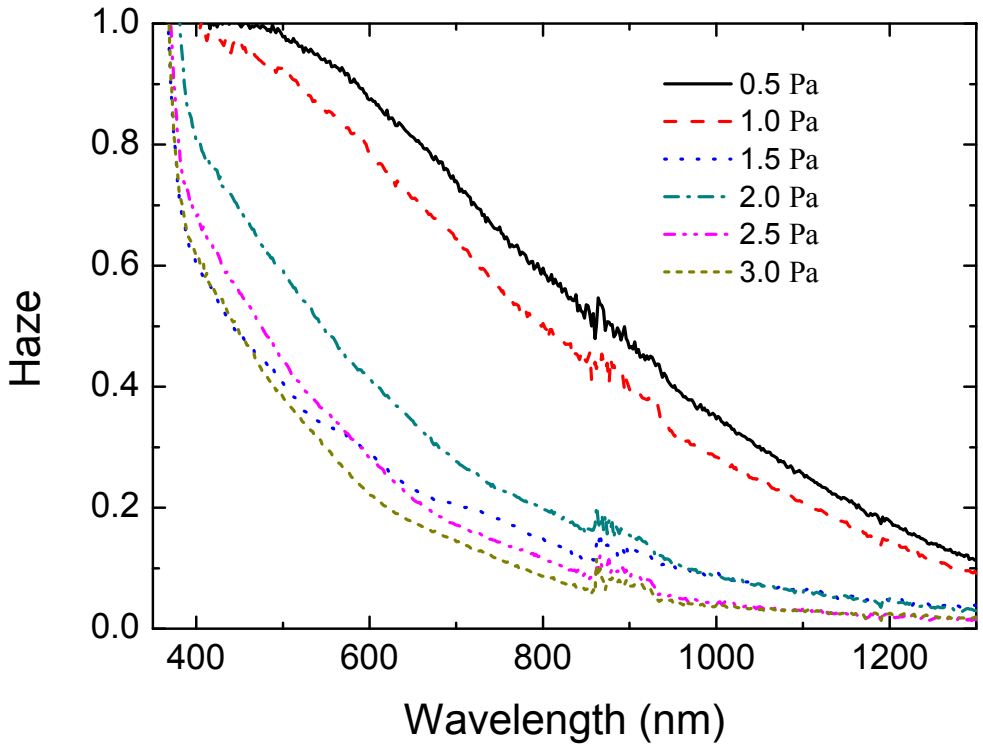
Haze
Wavelength (nm)
0.5 Pa
1.0 Pa
1.5 Pa
2.0 Pa
2.5 Pa
3.0 Pa
0.0
0.2
0.4
0.6
0.8
1.0
400
600
800
1000
1200

Zhu_Fig. 10

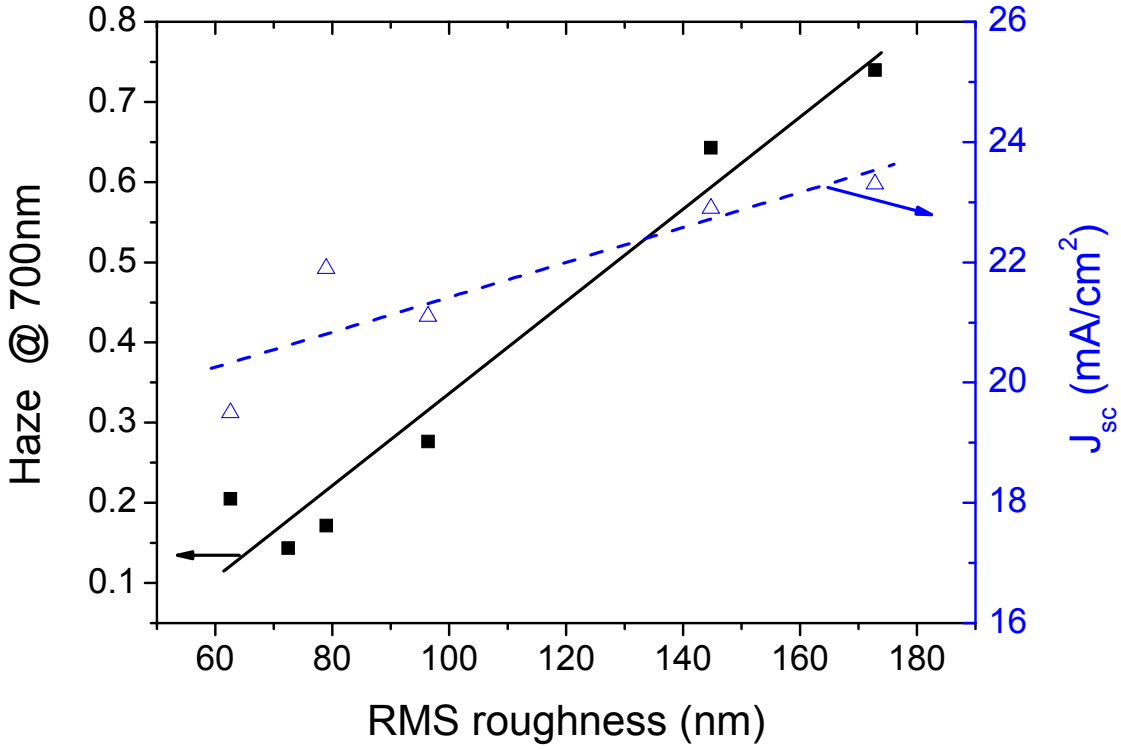
Haze @ 700nm
J_{sc} (mA/cm^2)
RMS roughness (nm)
0.8
0.7
0.6
0.5
0.4
0.3
0.2
0.1
26
24
22
20
18
16
60
80
100
120
140
160
180

Zhu_Fig. 11

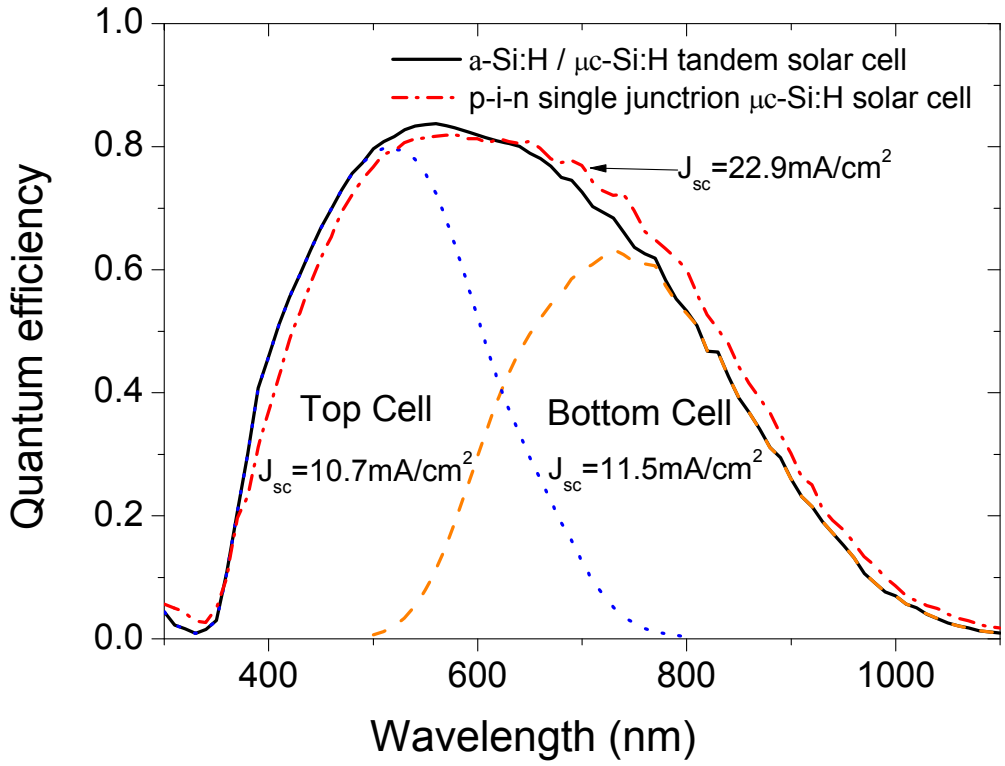
a-Si:H / μc-Si:H tandem solar cell
p-i-n single junctrion μc-Si:H solar cell
J_sc=22.9mA/cm^2
Top Cell
J_sc=10.7mA/cm^2
Bottom Cell
J_sc=11.5mA/cm^2
Quantum efficiency
Wavelength (nm)
1.0
0.8
0.6
0.4
0.2
0.0
400
600
800
1000

Zhu_Table 1.

Samples (Pa)	η (%)	FF (%)	V_{oc} (V)	J_{SC} (mA/cm^2)
0.5	8.4	70.4	0.511	23.3
1.0	8.5	71.4	0.518	22.9
1.5	7.4	72.1	0.521	19.5
2.0	6.9	65.3	0.496	21.1
2.5	7.0	64.4	0.492	21.9
1.0 (Tandem)	10.2	67.5	1.40	10.7